On Improving the Potential Field Method for Ring Formation*

Dzung Tran†, David W. Casbeer‡Isaac E. Weintraub‡, and Dejan Milutinović§

***Abstract*— In the ring formation control problem, the follower is designated to approach a ring defined relative to the leader. This type of formation gives the follower more flexibility as it trails the leader. To achieve such formation, the follower's reference velocity is derived using the potential field method, and then a sliding surface is constructed to enforce the follower to track the reference. Motivated by the Levenberg-Marquardt algorithm, this paper proposes modifications on the potential field method to further enhance the follower's performance in the ring formation. Specifically, adding the approximated Hessian into the formulation of the potential field has a damping effect on the controller and improves the follower's performance by reducing oscillations about the sliding surface. The use of the approximated Hessian, which is introduced in this paper in the context of ring formation, extends and is useful for control design of potential field methods in general. The proposed algorithm is discussed and interpreted from the feedback control viewpoint, where stability is guaranteed. A numerical example is also presented to illustrate the efficacy of the proposed algorithm.**

I. Introduction

This paper contributes to the studies in leader-wingman 3D formation where the leader governs the movement of the overall formation while the follower(s) tries to maintain a relative distance with respect to the leader [1]–[3]. Conventional leader-wingman formations confine the follower to a single desired position relative to the leader. For enabling more flexibility in the follower's motion, the ring formation control problem [4]–[6] extends the leader-wingman formation by calling for control algorithms for the follower to approach and maintain a position on a desired ring, which is a set of desired points defined relative to the leader.

The potential field method (see, for example, [7]–[9] and references therein) is an excellent tool for dealing with such problems. Specifically, the set of desired points can be defined using objective functions, from which the potential function is constructed. Subsequently, the potential field is often derived in the form of the gradient descent to drive the follower toward the desired points. This has been done in our previous work [4] where the follower was modeled with single-integrator kinematics. We then extended the follower's dynamics to a double integrator with saturation constraints on the control input in [6]. In particular, the potential field method was first used to generate the reference velocity, then a sliding surface was constructed to enforce the follower to track the reference velocity. Under the proposed algorithm in [6], we observed an oscillatory behavior in the follower's position as it approached the ring. This oscillation is a well-known limitation of the gradient descent when the minima (either local or global) are located at the ravine-like region as illustrated in Figure 1.

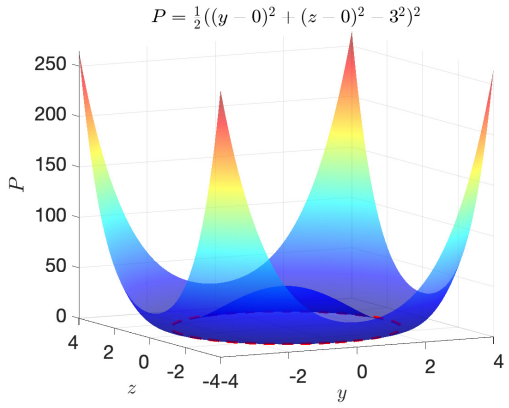

Figure 1. An illustration of a potential function with a ravine-like region, where the dashed line denotes the global minimum.

The Levenberg-Marquardt algorithm [10], [11] is a robust method for solving nonlinear least squares problem with many applications in robotics. For example, it is used in [12]–[14] for addressing the kinematic singularities of robotic manipulators. In addition, the authors of [15] utilize the Levenberg-Marquardt to reduce the oscillations of mobile robots when they are close to obstacles or in narrow passages. Motivated by the method, we aim to enhance the proposed result of [6]. In particular, the contributions of this paper are twofold: *i)* The approximated Hessian is introduced into the potential field formulation to generate the reference velocity and the sliding mode method is utilized to drive the follower's velocity to the reference value. We also show how to appropriately select the weighting coefficients for improving the overall performance. The improvement in the follower's performance is then validated through illustrative examples, which show that under the proposed algorithm there is no oscillation when the follower approaches the desired ring. *ii)* We provide discussion and explanation for the improvement from the feedback control viewpoint. Specifically, we show that by adding the approximated Hessian, the gradient descent is damped. We also remark that the control design approach described in this work can be applied to other region-based problems where a set of desired points can be established using objective functions.

The organization of this paper is as follows. The necessary mathematical preliminaries and the problem formulation are introduced in Sections II and III, respectively. In Section IV, the control architecture is proposed along with the stability analysis, and discussion on the effect of adding the approximated Hessian to the potential field formulation is presented. Illustrative numerical examples are provided in Section V to demonstrate the efficacy of the proposed control architecture. Finally, concluding remarks are summarized in Section VI.

†D. Tran is a Research Associate at Control Science Center, U.S. Air Force Research Laboratory, Wright-Patterson Air Force Base, OH 45433.

‡D. Casbeer and I. Weintraub are with the Control Science Center, U.S. Air Force Research Laboratory, Wright-Patterson Air Force Base, OH 45433.

§D. Milutinović is a Professor of the Department of Electrical and Computer Engineering at University of California Santa Cruz, Santa Cruz, CA 95064.

* Approved for public release: distribution unlimited, case number: AFRL-2021-2881. This work has been supported in part by AFOSR Grant 21RQCOR084.

II. Mathematical Preliminaries

The notations used in this paper are fairly standard. Specifically, $\mathbb{N}$ denotes the set of nonnegative integers, $\mathbb{R}$, $\mathbb{R}^n$, and $\mathbb{R}^{n\times m}$ respectively denote the set of real numbers, $n\times 1$ real column vectors, and $n\times m$ real matrices. We write $(\cdot)^{\mathrm{T}}$ for transpose of a vector or of a matrix, $(\cdot)^{-1}$ for the inverse of a nonsingular matrix, $\|\cdot\|_2$ for the Euclidean norm of a vector or induced two-norm of a matrix, and $\lambda_i(M)$ for the i-th eigenvalue of matrix M. A position or velocity vector without a superscript (e.g., p_f or v_f) indicates the vector is defined in the inertial frame; a position or velocity vector with a superscript (e.g., $p_f^{\mathcal{X}}$ or $v_f^{\mathcal{X}}$) indicates the vector is defined in the reference frame $\mathcal{X}$. Furthermore, a rotation matrix $\mathcal{R}_{\mathcal{X}}^{\mathcal{Y}}$ denotes a transformation from the reference frame $\mathcal{X}$ to the reference frame $\mathcal{Y}$.

The following lemmas are necessary for the development of the main result of the paper.

Lemma 1 (**Fact 2.16.26, [16]**). *Let $A, B \in \mathbb{R}^{n\times n}$, and assume that A and $A+B$ are nonsingular. Then, for all $k\in\mathbb{N}$,*

$$(A+B)^{-1} = \textstyle\sum_{i=0}^{k} A^{-1}(-BA^{-1})^i + (-A^{-1}B)^{k+1}(A+B)^{-1}. \tag{1}$$

Lemma 2 (**Section 5.2.4, [17]**). *Let $A\in\mathbb{R}^{n\times n}$ be a symmetric matrix, then its eigenvalues are real and $\lambda_i(A - c\mathrm{I}_n) = \lambda_i(A) - c$ for all $i = 1,\dots,n$ and $c\in\mathbb{R}$.*

III. Problem Formulation

Figure 2 shows a system consisting of two vehicles, a leader and a follower, is considered. The leader and the follower are free to move in 3-dimensional Cartesian space. The follower attempts to approach any position on a ring of radius $R\in\mathbb{R}_+$ behind the leader. Our goal is to design a controller that allows the follower to reach the ring and stay on it during the mission while the leader can freely navigate. For that purpose, we define $p_l \triangleq [p_{lx}, p_{ly}, p_{lz}]^{\mathrm{T}} \in \mathbb{R}^3$ and $p_f \triangleq [p_{fx}, p_{fy}, p_{fz}]^{\mathrm{T}} \in \mathbb{R}^3$ as positions of the leader and the follower in the inertial frame, respectively. The follower is subject to the double integrator dynamics given by

$$\dot{p}_f(t) = v_f(t), \tag{2}$$
$$\dot{v}_f(t) = u(t), \tag{3}$$

where $v_f(t)\in\mathbb{R}^3$ is the velocity of the follower and $u(t)\in\mathbb{R}^3$ is the control input satisfying the saturation constraints $|u_x|\le\bar{u}_x$, $|u_y|\le\bar{u}_y$, $|u_z|\le\bar{u}_z$ with $\bar{u}_x,\bar{u}_y,\bar{u}_z\in\mathbb{R}_+$. We also assume that the velocities and accelerations of the leader and the follower are bounded. As Figure 2 illustrates, we have

$$\mathcal{R}_i^L(\gamma,\chi)(p_f(t)-p_l(t)) = \mathcal{R}_i^L(\gamma,\chi)p_d(t) = p_f^L(t), \tag{4}$$

or equivalently,

$$p_f(t) = p_l(t) + \mathcal{R}_L^i(\gamma,\chi)p_f^L(t), \tag{5}$$

where the superscripts and subscripts i and L denote the inertial frame and the leader frame, respectively; $p_d(t) \triangleq p_f(t) - p_l(t)$ denotes the vector $\overrightarrow{LF}$ in the inertial frame, $p_f^L(t)$ is the position of the follower in the leader frame (i.e., the vector $\overrightarrow{LF}$ in the leader frame); γ and χ are the leader's flight path angle and course angle, respectively (see Figure 2); $\mathcal{R}_L^i(\gamma,\chi)$ is the rotation matrix for the transformation from the leader frame to inertial frame defined by (see, for example, [18, Chapter 2.4])

$$\mathcal{R}_L^i(\gamma,\chi) \triangleq \begin{bmatrix}\cos(\chi) & -\sin(\chi) & 0\\ \sin(\chi) & \cos(\chi) & 0\\ 0 & 0 & 1\end{bmatrix}\begin{bmatrix}\cos(\gamma) & 0 & \sin(\gamma)\\ 0 & 1 & 0\\ -\sin(\gamma) & 0 & \cos(\gamma)\end{bmatrix}. \tag{6}$$

We note that $\big(\mathcal{R}_i^L(\gamma,\chi)\big)^{-1} = \big(\mathcal{R}_i^L(\gamma,\chi)\big)^{\mathrm{T}} = \mathcal{R}_L^i(\gamma,\chi)$. Let $c^L \triangleq [c_x^L, c_y^L, c_z^L]^{\mathrm{T}} \in \mathbb{R}^3$ be the center of the ring and $r^{*L}\in\mathbb{R}^3$ be an arbitrary vector in the set of vectors representing the ring in the leader frame, which is illustrated by the dashed circle in Figure 2. In other words, we want to achieve $p_f(t) = p_l(t) + \mathcal{R}_L^i(\gamma,\chi)r^{*L}$.

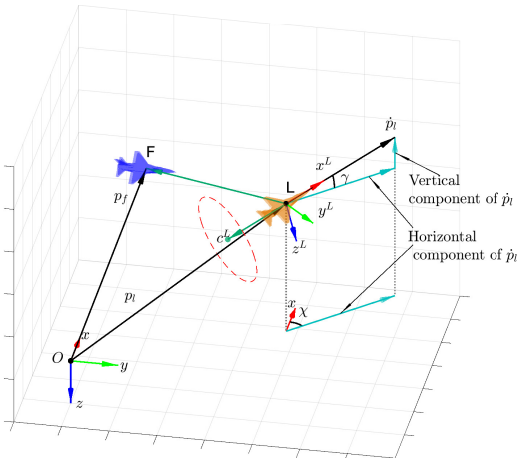

Figure 2. An illustration of vectors in the inertial frame (black) and the leader body frame (jade) where the leader is located at L, the follower is located at F, and the center of the ring is located at the tip of $c^L\in\mathbb{R}^3$.

IV. Ring Formation Maneuver with Potential Field Method

In this section, we propose a control design procedure for achieving the ring formation. In particular, we first define the ring through objective functions and construct the potential function. Next, the follower's reference velocity is generated from the potential field. Then, a sliding mode controller is designed to enforce the follower's velocity to track the reference velocity. For that purpose, we start with the definition of the following objective functions

$$f_1(p_d) \triangleq (p_{dx} - [\mathcal{R}_L^i(\gamma,\chi)c^L]_x)^2, \tag{7}$$
$$f_2(p_d) \triangleq (p_{dy} - [\mathcal{R}_L^i(\gamma,\chi)c^L]_y)^2 + (p_{dz} - [\mathcal{R}_L^i(\gamma,\chi)c^L]_z)^2 - R^2, \tag{8}$$

where p_{di} and $[\mathcal{R}_L^i(\gamma,\chi)c^L]_j$ with $j = x,y,z$ are the components of p_d and $\mathcal{R}_L^i(\gamma,\chi)c^L$, respectively. The follower is on the desired ring when the aforementioned objective functions both approach zero; that is, r^{*L} is defined implicitly by $f_1(p_d) = f_2(p_d) = 0$. Therefore, we need to derive a reference velocity for driving the objective functions to zero. For that purpose, let $f \triangleq [f_1, f_2]^{\mathrm{T}}$ be the vector of objective functions, we now construct the potential function, which

plays Lyapunov-like role, as

$$V_1(p_d) = \frac{1}{2} f^{\mathrm{T}} f. \tag{9}$$

As an illustration of the potential field in yz plane, Figure 1 depicts the potential generated from the objective function (8) with $R = 3$. The gradient is then obtained from taking the partial derivative of $V_1(p_d)$ with respect to p_d

$$\begin{aligned}\frac{\partial V_1}{\partial p_d} &= \left(\frac{\partial f}{\partial p_d}\right)^{\mathrm{T}} \left(\frac{\partial V_1}{\partial f}\right) \\ &= \underbrace{\begin{bmatrix} (p_{dx} - [\mathcal{R}_L^i(\gamma,\chi)c^L]_x) & 0 \\ 0 & (p_{dy} - [\mathcal{R}_L^i(\gamma,\chi)c^L]_y) \\ 0 & (p_{dz} - [\mathcal{R}_L^i(\gamma,\chi)c^L]_z) \end{bmatrix}}_{J(p_d)^{\mathrm{T}}} \begin{bmatrix} f_1 \\ f_2 \end{bmatrix} \\ &= J(p_d)^{\mathrm{T}} f, \end{aligned} \tag{10}$$

where $J(p_d) \triangleq \frac{\partial f}{\partial p_d} \in \mathbb{R}^{2\times 3}$ is the Jacobian matrix. The most common way to construct the potential field is to follow the gradient descent and set the reference velocity to $v_{f_{ref}}(t) = -\frac{\partial V_1}{\partial p_d} = -J(p_d)^{\mathrm{T}} f$. This has been done in our earlier studies [4] and [6], however, one disadvantage of utilizing the gradient descent in feedback control is that the gradient is large if the vehicle is far from the set of desired points and therefore causes aggressive behavior. Furthermore, if the set of desired points is in a ravine-like region (see, for example, Figure 1), the vehicle would oscillate before settling at the desired points.

A. The proposed reference velocity

To avoid undesired behaviors and being motivated by the Levenberg-Marquardt algorithm [10] and [11], we propose

$$\dot{p}_d(t) = v_{f_{ref}}(t) \triangleq -(\mu_1 \mathrm{I}_3 + \mu_2 H)^{-1} J^{\mathrm{T}} f, \tag{11}$$

or equivalently,

$$\dot{p}_f(t) = v_{f_{ref}}(t) + \dot{p}_l, \tag{12}$$

where $J = J(p_d)$, and $H \triangleq J^{\mathrm{T}} J \in \mathbb{R}^{3\times 3}$ is the approximated Hessian, which is symmetric and positive semidefinite[1]; μ_1 and $\mu_2 \in \mathbb{R}_+$ denote positive gains. The following lemma is necessary for the development of the main result.

Lemma 3. *The matrix $M \triangleq \mu_1 \mathrm{I}_3 + \mu_2 H$ is positive definite.*

This lemma comes directly from the fact that H and I_3 are symmetric matrices and Lemma 2. We now can state the following theorem.

Theorem 1. *If the follower velocity follows the dynamics given by (12), then the follower either approaches the center of the ring or the ring.*

Proof. Consider the Lyapunov-like function (9), then its time derivative along the trajectory of (11) is given by

$$\begin{aligned}\dot{V}_1(\cdot) &= \left(\frac{\partial V_1}{\partial p_d}\right)^{\mathrm{T}} \left(\frac{\partial p_d}{\partial t}\right) \\ &= -(J^{\mathrm{T}} f)^{\mathrm{T}} (\mu_1 \mathrm{I}_3 + \mu_2 H)^{-1} (J^{\mathrm{T}} f) \le 0, \end{aligned} \tag{13}$$

[1]This comes directly from the fact that our specified J matrix has $\operatorname{rank} J^{\mathrm{T}} = \operatorname{rank} J^{\mathrm{T}} J = \operatorname{rank} H \le 2$, and the matrix $J^{\mathrm{T}} J$ is symmetric with nonnegative eigenvalues.

where the last inequality comes directly from Lemma 3. Next, consider the set $\Omega \triangleq \{p_d \in \mathbb{R}^3 : V_1(p_d) \le d\}$ where d is some positive constant. If $p_d(0) \in \Omega$, it follows from (13) that $p_d(t)$ remains in Ω for all $t > 0$. Thus, Ω is a compact set. By LaSalle's invariance principle (see, for example [19, Chapter 3.4]), every solution starting in Ω approaches the largest invariant set in $E = \{p_d \in \mathbb{R}^3 : \dot{V}_1 = 0\}$. Note that since the matrix $\mu_1 \mathrm{I}_3 + \mu_2 H$ is positive definite, the last inequality in (13) indicates $\dot{V}_1 = 0$ only when $J^{\mathrm{T}} f = 0$; that is, (i) $f_1(p_d)(p_{dx} - [\mathcal{R}_L^i(\gamma,\chi)c^L]_x) = 0$, (ii) $f_2(p_d)(p_{dy} - [\mathcal{R}_L^i(\gamma,\chi)c^L]_y) = 0$ and (iii) $f_2(p_d)(p_{dz} - [\mathcal{R}_L^i(\gamma,\chi)c^L]_z) = 0$, simultaneously. In other words, $E = \mathcal{R}_L^i(\gamma,\chi)c^L \cup \{p_d \in \mathbb{R}^3 : f_1(p_d) = f_2(p_d) = 0\}$, which is the center of the ring and the ring. Since both component sets of E are invariant, the largest invariant set in E is itself. In addition, $V_1(p_d)$ is radially unbounded and hence all trajectories converge to either the center of the ring or the ring. ■

Remark 1. The center of the ring in the inertial frame $\mathcal{R}_L^i(\gamma,\chi)c^L$ is an unstable equilibrium point, and hence, any perturbation and/or disturbance (e.g., winds) about this point makes p_f^L move away from it and converge to the ring. The follower therefore does not pragmatically converge to the center of the ring.

B. Constructing the Controller

Next, to design the controller $u(t)$ subjected to the saturation constraints for the double integrator dynamics given by (2)-(3), we define

$$s(t) \triangleq \dot{p}_d(t) - v_{f_{ref}}(t) + \xi(t) \in \mathbb{R}^3, \tag{14}$$

where $\xi(t) \in \mathbb{R}^3$ is an extra term to compensate for the input saturation and is updated under the dynamics given by

$$\dot{\xi}(t) = -k\xi(t) + \Delta u(t), \qquad \xi(0) = \xi_0, \tag{15}$$

where $k \in \mathbb{R}_+$ is a constant gain, $\Delta u(t) \triangleq u_d(t) - u_a(t)$ with $u_d(t) \triangleq [u_{dx},\ u_{dy},\ u_{dz}]^{\mathrm{T}}$ being the designed controller and $u_a(t)$ being the saturated controller defined by

$$u_a(t) \equiv u(t) \triangleq \mathrm{sat}(u_d) = [\mathrm{sat}(u_{dx}),\ \mathrm{sat}(u_{dy}),\ \mathrm{sat}(u_{dz})]^{\mathrm{T}}. \tag{16}$$

Once again, $\mathrm{sat}(u_{di}) = \mathrm{sign}(u_{di}) \min\{|u_{di}|, \bar{u}_i\}$ for $i = x, y, z$. In general, the initial value ξ_0 can be set to any finite value, yet it is often set to zero. We want to design the controller to bring the trajectory to the sliding manifold $s = 0$ and maintain it there. Toward that end, taking the time derivative of (14) yields

$$\begin{aligned}\dot{s}(t) &= u(t) - \ddot{p}_l(t) - \dot{v}_{f_{ref}}(t) - k\xi(t) + \Delta u(t) \\ &= u_d(t) - \ddot{p}_l(t) - \dot{v}_{f_{ref}}(t) - k\xi(t), \end{aligned} \tag{17}$$

where $\ddot{p}_l(t)$ and $\dot{v}_{f_{ref}}(t)$ can be obtained by passing $p_l(t)$ and $v_{f_{ref}}(t)$ through command filters (see, for example, [20], [21]). Note that the command filter contains magnitude limiter and rate limiter; therefore, $\ddot{p}_l(t)$ and $\dot{v}_{f_{ref}}(t)$ can be bounded when necessary. We now select the Lyapunov function candidate

$$V_2 = \frac{1}{2} s^{\mathrm{T}} s, \tag{18}$$

and take its time derivative along the trajectory (17) to obtain

$$\dot{V}_2 = s^{\mathrm{T}} \left(u_d(t) - \ddot{p}_l(t) - \dot{v}_{f_{ref}}(t) - k\xi(t) \right). \tag{19}$$

By choosing the controller

$$u_d(t) = \ddot{p}_l(t) + \dot{v}_{f_{ref}}(t) + k\xi(t) - k_2 s(t) - k_3 \operatorname{sign}(s), \tag{20}$$

with $k_2, k_3 \in \mathbb{R}_+$ being constant gains and $\operatorname{sign}(s) = [\operatorname{sign}(s_x),\ \operatorname{sign}(s_y),\ \operatorname{sign}(s_z)]^{\mathrm{T}}$, (19) becomes

$$\begin{aligned} \dot{V}_2 =& - k_2 s^{\mathrm{T}} s - k_3 s^{\mathrm{T}} \operatorname{sign}(s) \\ \leq& - k_3 \|s\|_1 = -k_3 \left(|s_x| + |s_y| + |s_z| \right). \end{aligned} \tag{21}$$

With the preceding procedure, the main result of this section can be expressed the following theorem.

Theorem 2. *Consider the follower's double integrator dynamics given by (2)-(3), and the reference vector r^{L*}, which is implicitly defined by the objective functions (7)-(8) when $f_1(p_d) = f_2(p_d) = 0$. If the follower executes the controller $u_a(t)$, which is constructed following the controller design procedure shown by (9-21) with $u_d(t)$ given by (20), and no input saturation occurs after finite time, then the follower converges to the desired ring.*

Proof. With the Lyapunov function (18) and its time derivative (21), it is guaranteed that the trajectories reach the manifold $s = 0$ in finite time (see, for example, [19, Chapter 10.1]). In addition, we assume that no input saturation occurs after finite time; that is, there exists a finite time $\tau \in \mathbb{R}_+$ such that $\Delta u(t) = 0$ for $t \geq \tau$. As a result, the dynamics (15) indicates the compensative term $\xi(t)$ exponentially converges to 0 for $t > \tau$. Since $s(t) = \dot{p}_d - v_{f_{ref}}(t) + \xi$, when $s(t)$ and $\xi(t)$ approach 0, $\dot{p}_d(t)$ approaches $v_{f_{ref}}(t)$, which drives the follower to the desired ring as shown in Theorem 1 and discussed in Remark 1. ■

C. Damping Effect of the Proposed Reference Velocity

In our previous works [4] and [6], the effects of a large gradient were mitigated by using the natural logarithm and hyperbolic functions for constructing the potential functions instead of putting it in the least squares form. In this paper, the least squares form of the potential field (9) is utilized and the proposed reference velocity given by (11) is based on the Levenberg-Marquardt method, which introduces the approximated Hessian into the dynamics. We note that in solving nonlinear least squares problems, the Levenberg-Marquardt method is well known for its fast convergence and is often seen with $\mu_2 = 1$ and μ_1 is an adaptive term. In this work, we set μ_1 and μ_2 to constant gains and look at the Levenberg-Marquardt method from the feedback control perspective. Especially, we want to emphasize the damping effect of the structure (11), which helps improve the performance of the overall system. Stated more specifically, using Lemma 1 with $A = \mu_1 \mathrm{I}_3$, $B = \mu_2 H$, and $k = 0$, then we have

$$\begin{aligned} M^{-1} =& (\mu_1 \mathrm{I}_3 + \mu_2 H)^{-1} = \frac{1}{\mu_1}\mathrm{I}_3 - \frac{\mu_2}{\mu_1} H (\mu_1 \mathrm{I}_3 + \mu_2 H)^{-1} \\ =& \frac{1}{\mu_1}\mathrm{I}_3 - \frac{\mu_2}{\mu_1} H M^{-1}. \end{aligned} \tag{22}$$

As a result, (11) can be rewritten in the form

$$\begin{aligned} \dot{p}_d(t) =& - \left(\mu_1 \mathrm{I}_3 - \mu_2 H M^{-1} \right) J^{\mathrm{T}} f \\ =& - \frac{1}{\mu_1} J^{\mathrm{T}} f + \frac{\mu_2}{\mu_1} H M^{-1} J^{\mathrm{T}} f, \end{aligned} \tag{23}$$

where the first term is the gradient descent and the second term is the damping term of the gradient descent, which is proved shortly. We start with the following lemma.

Lemma 4. *The matrix HM^{-1} is positive semidefinite.*

Proof. Utilizing (22) yields

$$H M^{-1} = \frac{1}{\mu_2}\mathrm{I}_3 - \frac{\mu_1}{\mu_2} M^{-1}, \tag{24}$$

and hence, HM^{-1} is symmetric. From Lemma 2, one obtains $\lambda_i(M) = \mu_1 + \mu_2 \lambda_i(H) > 0$ for all $i = 1, 2, 3$, and

$$\begin{aligned} \lambda_i(HM^{-1}) =& \frac{1}{\mu_2} - \frac{\mu_1}{\mu_2} \left(\frac{1}{\mu_1 + \mu_2 \lambda_i(H)} \right) \\ =& \frac{\lambda_i(H)}{\mu_1 + \mu_2 \lambda_i(H)}, \quad \forall\ i = 1, 2, 3. \end{aligned} \tag{25}$$

Since $\lambda_i(H) \geq 0$ and $\mu_1 + \mu_2 \lambda_i(H) > 0$, $\lambda_i(HM^{-1}) \geq 0$ for all $i = 1, 2, 3$. The result is now immediate. ■

Proposition 1. *The term "$\frac{\mu_2}{\mu_1} HM^{-1} J^{\mathrm{T}} f$" in (23) is the damping term of the gradient descent.*

Proof. Taking the dot product of the first and second term in (23) and utilizing Lemma 4 yield

$$\begin{aligned} p \triangleq& \left(-\frac{1}{\mu_1} J^{\mathrm{T}} f \right)^{\mathrm{T}} \left(\frac{\mu_2}{\mu_1} H M^{-1} J^{\mathrm{T}} f \right) \\ =& - \frac{\mu_2}{\mu_1^2} \left(J^{\mathrm{T}} f \right)^{\mathrm{T}} H M^{-1} (J^{\mathrm{T}} f) \leq 0. \end{aligned} \tag{26}$$

This indicates that the vector "$\frac{\mu_2}{\mu_1} HM^{-1} J^{\mathrm{T}} f$" always belongs to the an opposite half-space of the gradient descent (i.e., the first term in (23)). Hence, the result follows. ■

D. Discussion of the performance

Since $(\mu_1 \mathrm{I}_3 + \mu_2 H)^{-1}$ is positive definite, the result vector of (23) is in the same half-space with the gradient descent. Consequently, the gain μ_2 can be set to an arbitrarily large value. The damping effect of the proposed reference velocity (11) will be illustrated in Section V. In addition, let $\dot{\tilde{V}}_1(\cdot) = -(J^{\mathrm{T}} f)^{\mathrm{T}} (\mu_1 \mathrm{I}_3)^{-1} (J^{\mathrm{T}} f) \leq 0$ being the time derivative of the the Lyapunov-like function (9) corresponding to $\mu_2 = 0$ (i.e., the reference velocity is the gradient descent), then from (13) and (22), one can easily justify that

$$\dot{V}_1(\cdot) - \dot{\tilde{V}}_1(\cdot) = -\mu_1 p \geq 0, \tag{27}$$

where p is given in (26). Therefore, under (11), $V_1(p_d)$ approaches zero slower than the reference velocity generated by the gradient descent method. This results from the damping term. We note that in general the magnitude of the gradient descent is quadratically proportional to the distance to the ring. As a result, the reference velocity generated by the gradient descent method has the tendency to change drastically when the follower approaches the ring, whereas it takes time for the acceleration to drive the follower velocity toward the reference. This causes not only the acceleration (i.e., the control input) to be saturated but also oscillations when the

follower is in the vicinity of the ring as the potential field around the ring is ravine-like (see Figure 1 for illustration). On the other hand, with an appropriate choice of μ_1 and μ_2 for the proposed reference velocity (11), the gradient descent can be damped and results in reference velocity vectors with moderate magnitudes, which can release the control input from being saturated as well as reduce oscillations.

While a good selection of μ_1 and μ_2 depends on the vehicle configurations and the saturation threshold of the control input, some trade-offs on varying these gains can be observed. A large value of μ_1 induces a reference velocity with a small magnitude, which can be achievable without making the control input saturated; however, the follower may converge to the ring slowly. On the other hand, a small value of μ_1 induces a reference velocity with a large magnitude, which could make the control input constantly saturated and results in oscillations when approaching the ring. In addition, for a fixed μ_1 value, if μ_2 is set to a large value, the result reference velocity vector is small, and a slow convergence can be expected. If μ_2 is set to a small value, the damping effect is mitigated.

V. Illustrative Numerical Examples

For this numerical example, the leader's and follower's initial positions are set to $[-300, -500, 1000]^{\mathrm{T}}$ and $[-350, -520, 1010]^{\mathrm{T}}$, respectively. The desired ring is chosen to have the radius $R = 10$ m and the center $c^L = [-10, 0, 0]^{\mathrm{T}}$. The leader is commanded to travel on a straight line at a constant speed of 30 m/s while the follower has an initial speed of 25 m/s. The proposed controller $u_a(t)$ (16) is implemented with $u_d(t)$ being given by (20) and $\bar{u} = [10, 5, 5]^{\mathrm{T}}$. In addition, the constant gains are set to $k_1 = 0.5$, $k_2 = 2$, $k_3 = 1$, and the term $\mathrm{sign}(s)$ is replaced by $\tanh(5s)$ to prevent the chattering of the control signal.

For comparison purposes, we implement the reference velocity (11) under two different configurations. For the first case, we set $\mu_1 = 10$ and $\mu_2 = 0$ and impose a saturation constraint on the reference velocity to prevent it from growing large.[2] For the second case, we set $\mu_1 = 10$ and $\mu_2 = 2$ with no saturation constraint on the reference velocity. Figures 3-5 show the performance of the follower for these two cases. In particular, Figure 3 shows that the trajectories of the follower (blue aircraft) converge to the desired ring in both case. However, the trajectory of the first case (dotted line) oscillates as the vehicle approach the desired ring, whereas the trajectory of the second case (solid line) is smooth. In addition, the oscillations of the first case are also captured in the evolution of its f_2 (dash-dotted line) as illustrated in Figure 4. One can also observe in Figure 4 that f_1 and f_2 in the second case (solid lines) are smooth and represent a better convergence. Furthermore, the evolution of $\xi(t)$, $s(t)$ and $u(t)$ in the second case are plotted in Figure 5. Specifically, the controller is only saturated at the beginning due to a large initial error (or large values of f_1 and f_2), which leads to the initial growth of ξ. Yet, ξ quickly decays to zero, which indicates that the controller is no longer saturated afterward. The variable s also converges to a small neighborhood of zero indicating that $\dot{p}_d$ closely tracks to the reference velocity $v_{f_{ref}}$.

[2]Imposing a saturation constraint on the reference velocity still results in the convergence of the follower to the desired ring. We refer interested readers to [6] for the detailed proof.

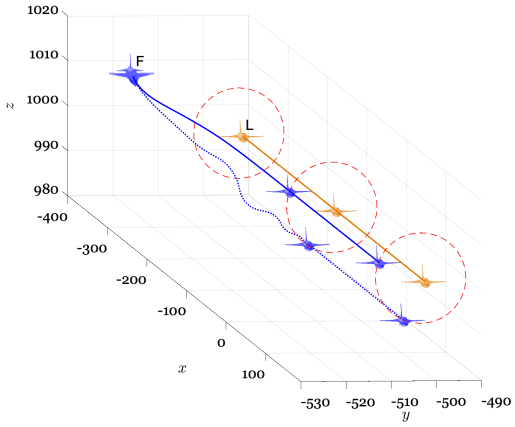

Figure 3. The evolution of the follower (blue aircraft) under the proposed algorithm (16) and the reference velocity (11) with $\mu_1 = 10$ and: (i) $\mu_2 = 0$ (dotted line) and (ii) $\mu_2 = 2$ (solid line).

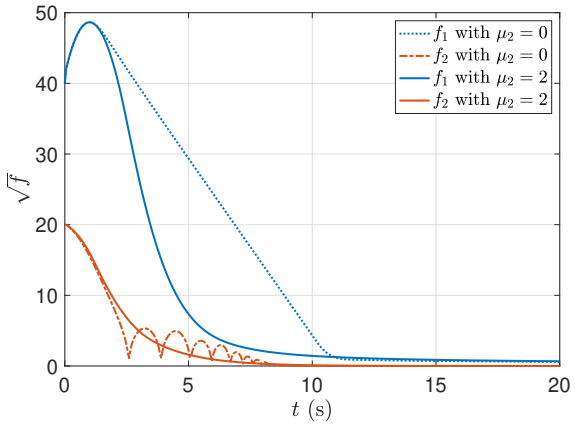

Figure 4. The evolution of $\sqrt{|f_1(p_d)|}$, $\sqrt{|f_2(p_d)|}$ where f_1 and f_2 are defined in (7) and (8) under the reference velocity (11) with $\mu_1 = 10$ and: (i) $\mu_2 = 0$ (dotted and dashed lines) and (ii) $\mu_2 = 2$ (solid lines).

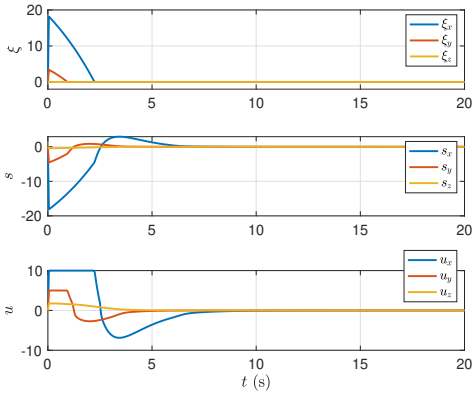

Figure 5. The evolution of $\xi(t)$ (top), $s(t)$ (middle) and $u(t)$ (bottom) under the proposed algorithm (16) and the reference velocity (11) with $\mu_1 = 10$ and $\mu_2 = 2$..

To further illustrate the effectiveness of the proposed controller, the configurations in the above second case (i.e., $\mu_1 = 10$ and $\mu_2 = 2$) for the follower controller is used for a highly maneuverable scenario. In particular, the leader and follower are initially positioned at $[-300, -500, 1000]^{\mathrm{T}}$ and $[-320, -550, 1050]^{\mathrm{T}}$, respectively. The leader is commanded

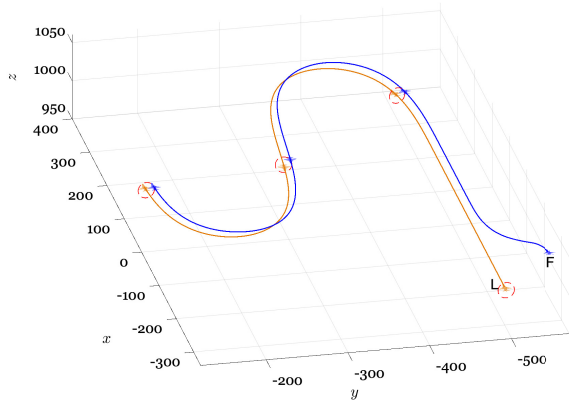

Figure 6. The evolution of the follower under the proposed algorithm (16) and the reference velocity (11) with $\mu_1 = 10$ and $\mu_2 = 2$, where the leader follows an S-shaped trajectory.

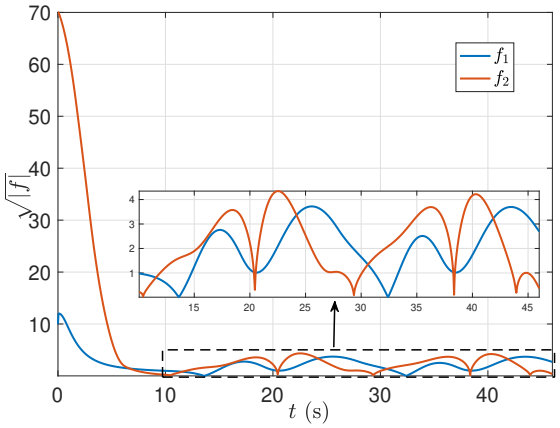

Figure 7. The evolution of $\sqrt{|f_1(p_d)|}$, $\sqrt{|f_2(p_d)|}$ where f_1 and f_2 are defined in (7) and (8) under the reference velocity (11) with $\mu_1 = 10$ and $\mu_2 = 2$, where the leader follows an S-shaped trajectory.

to follow a fixed-altitude S-shaped trajectory. The performance of the follower under the proposed controller is demonstrated in Figures 6 and 7. More details, Figures 6 shows that the follower is able to approach the ring smoothly without oscillations. Figures 7 shows that f_1 and f_2 quickly converge to zero neighborhood, and therefore, the follower can closely track the leader during the mission in spite of the highly maneuverable trajectory. It can be also observed in Figure 6 that the ring formation allows the follower to shift from right to left with relative to the leader, and vice versa, during the mission depending on the movement of the leader.

VI. Conclusion

The paper proposed to add the approximated Hessian into the potential field formulation for improving the follower's performance in the ring formation. It has been shown that with this addition, the gradient descent is damped and allows for the follower to converge to the desired ring without oscillations. The improvement was validated through the examples. For the future work, we will investigate designing a distributed controller for multiple followers to converge to the ring as well as implementing collision avoidance among the vehicles.

References

[1] L. Buzogany, M. Pachter, and J. D'azzo, "Automated control of aircraft in formation flight," in *AIAA Guidance, Navigation and Control Conference*, 1993.

[2] M. Pachter, J. J. D'Azzo, and J. L. Dargan, "Automatic formation flight control," *AIAA Journal of Guidance, Control, and Dynamics*, vol. 17, no. 6, pp. 1380–1383, Nov. 1994.

[3] V. P. Reyna, "Automation of formation flight control," Ph.D. dissertation, Air Force Institute of Technology, 1994.

[4] D. M. Tran, D. Casbeer, E. Garcia, I. E. Weintraub, D. Milutinovic, and S. G. Manyam, "Ring formation maneuver: Single-integrator kinematics," in *AIAA Scitech Forum*, 2021, p. 0978.

[5] D. Tran, D. Casbeer, E. Garcia, I. E. Weintraub, and D. Milutinović, "Ring formation maneuvering with double integrator dynamics," in *IEEE International Conference on Unmanned Aircraft Systems*, 2021, pp. 1580–1586.

[6] D. Tran, D. Casbeer, E. Garcia, I. E. Weintraub, and D. Milutinović, "Ring formation maneuver: Double-integrator kinematics with input saturation," *AIAA Journal of Guidance, Control, and Dynamics*, 2021 (Accepted).

[7] L. Barnes, M. Fields, and K. Valavanis, "Unmanned ground vehicle swarm formation control using potential fields," in *IEEE Mediterranean Conference on Control & Automation*, 2007, pp. 1–8.

[8] S. Hou, C. Cheah, and J. Slotine, "Dynamic region following formation control for a swarm of robots," in *IEEE International Conference on Robotics and Automation*, 2009.

[9] D. J. Bennet, C. R. MacInnes, M. Suzuki, and K. Uchiyama, "Autonomous three-dimensional formation flight for a swarm of unmanned aerial vehicles," *AIAA Journal of Guidance, Control, and Dynamics*, vol. 34, no. 6, pp. 1899–1908, Nov. 2011.

[10] K. Levenberg, "A method for the solution of certain non-linear problems in least squares," *Quarterly of Applied Mathematics*, vol. 2, no. 2, pp. 164–168, 1944.

[11] D. W. Marquardt, "An algorithm for least-squares estimation of nonlinear parameters," *Journal of the Society for Industrial and Applied Mathematics*, vol. 11, no. 2, pp. 431–441, 1963.

[12] C. W. Wampler, "Manipulator inverse kinematic solutions based on vector formulations and damped least-squares methods," *IEEE Transactions on Systems, Man, and Cybernetics*, vol. 16, no. 1, pp. 93–101, 1986.

[13] S. Chiaverini, B. Siciliano, and O. Egeland, "Review of the damped least-squares inverse kinematics with experiments on an industrial robot manipulator," *IEEE Transactions on control systems technology*, vol. 2, no. 2, pp. 123–134, 1994.

[14] G. Palmieri and C. Scoccia, "Motion planning and control of redundant manipulators for dynamical obstacle avoidance," *Machines*, vol. 9, no. 6, p. 121, 2021.

[15] K. Biswas and I. Kar, "On reduction of oscillations in target tracking by artificial potential field method," in *IEEE International Conference on Industrial and Information Systems (ICIIS)*, 2014, pp. 1–6.

[16] D. S. Bernstein, *Matrix mathematics*. Princeton university press, 2009.

[17] K. B. Petersen and M. S. Pedersen, "The matrix cookbook," 2012.

[18] R. W. Beard and T. W. McLain, *Small Unmanned Aircraft: Theory and Practice*. Princeton university press, 2012.

[19] H. K. Khalil, *Nonlinear Control*. Pearson Higher Ed, 2014.

[20] J. Farrell, M. Sharma, and M. Polycarpou, "Backstepping-based flight control with adaptive function approximation," *AIAA Journal of Guidance, Control, and Dynamics*, vol. 28, no. 6, pp. 1089–1102, 2005.

[21] J. A. Farrell, M. Polycarpou, M. Sharma, and W. Dong, "Command filtered backstepping," *IEEE Transactions on Automatic Control*, vol. 54, no. 6, pp. 1391–1395, 2009.